AIAA JOURNAL
Vol. , No. ,

Slotted Waveguide Stress Concentration Factor

Joseph Brooks* and Robert A. Canfield†
Virginia Polytechnic Institute and State University, Blacksburg, Virginia 24061

https://doi.org/10.2514/1.J060864

Sharp turns or corners within a structure lead to local failures well before the rest of the structure due to the creation of stress concentrations. For a load-bearing waveguide, these occur at the corners of the slots. After modeling a test waveguide, a bivariate curve fit was created to model these stress concentrations, based on four configurations for a single slot length, then refined into a trivariate form based on an expanded eight cases across two slot lengths. Once properly formatted, the integration of the bivariate function into an optimization allowed stress concentration to be estimated at the slot corners within a coarse low-fidelity model, rather than the high-fidelity model otherwise required, following the expected behavior and acting as a verification case. Implementation of the full trivariate form into a design optimization enabled use of the concentration factor to estimate the critical stress. The study showed that the inset copper waveguide could not be loaded from the outset, and that an offset of the copper waveguide could avoid overloading it.

Nomenclature

A	=	Area
D	=	unreduced area
d	=	reduced area between slots
d_1	=	slot width
d_3	=	slot centerline offset
d_6	=	waveguide height
E_g	=	Young's modulus of graphite epoxy
G	=	shear modulus
K_t	=	concentration factor
P_{cr}	=	critical buckling load
P_e	=	Euler column buckling load
r	=	fillet radius
s	=	nearest slot corner distance
t_c	=	copper thickness
δ	=	copper end offset
σ_x	=	stress of type x

I. Introduction

THE overall shape of a structure under load can lead to certain areas having a higher stress than others. Often, these stress concentrations are the result of sudden changes in the structural layout, such as sharp turns, and act as the most likely failure points within a structure. As a result, it is important to estimate what the increased stresses will be to prevent any local failures that could lead to an overall compromise of the structure. Within a load-bearing slotted waveguide, these stress concentrations occur at the corners of the slots cut into the waveguide's surface. The ratio between this higher corner stress and the uniform stress away from the point of interest is defined as a concentration factor K_t and can be used to estimate the corner stress from a given uniform stress.

In linear elasticity theory, the stress at a sharp corner is singular and will tend to infinity. Nonetheless, no crack or corner is perfectly sharp, resulting in a measurable, but finite, stress increase. As a result, a rounded corner, or fillet, is usually introduced to limit stress at these points of interest. Elasticity solutions are rarely available for more than simple geometries, so the effects of the fillets are often studied by refining meshes of numerical models to best capture the behavior. Many widely used shapes are then generalized into an empirical curve-fit, such as those found in *Roark's Formulas for Stress and Strain*, which can be employed for design calculations. For the waveguide structure, Roark's type 5 fillet, as shown within the portion of Table 17.1 [1], replicated in Figs. 1 and 2, was used as a guide for expected results, due to the similarity between its shape and a filleted waveguide slot, except for a slot that would be caught within the central area of the equivalent Roark irregularity.

The concepts are based on earlier studies conducted by Kim and Canfield, in which multiple potential waveguide configurations were analyzed. Whereas some concepts kept the waveguide itself unloaded, others examined the idea of the waveguide itself bearing part of the load [2,3]. As such, the concentration factors caused by the slots are of interest, to ensure accurate low-fidelity structural models of the waveguide. These low-fidelity models will allow for designs to be compared against design requirements quickly and efficiently. The analysis herein began with a purely copper waveguide, finding an empirical curve fit for the waveguide slot stress concentration, before moving on to its role within a larger optimization and use within a composite design.

II. Concentration Factor Curve Fit

For a given waveguide, the dimensions that affect the overall shape are the individual width of each waveguide ($d_5 = 22.86$ mm), the thickness of the fiberglass sleeves encasing each waveguide ($t_f = 0.75$ mm), the varying slot width d_1, and slot centerline spacing d_3. These parameters and additional parameters used later can be seen in Fig. 3, with the waveguide layup shown on the left [4], the waveguide sleeve material thicknesses shown in transparency in the center, and the dimensions specific to the copper waveguide itself shown on the right. The nomenclature employed for the waveguide itself ($d_1 - d_6$) was adopted as a continuation of the nomenclature employed in Kim et al., whereas the design layup shown on the left corresponds to the fourth design in an earlier study by Kim et al. that examined their influence on electromagnetic performance [4].

A mesh convergence study was conducted to ensure the changes in stress concentrations were properly captured. Three meshes were tested, as shown in Fig. 4. The "fine" mesh had seven nodes along the curvature of the fillet and 4212 elements. The "finer" mesh increased the number of nodes on the fillet to eight. Further refinement from 5322 elements to 7900 elements in the "finest" mesh did not change the number of nodes along the fillet. The concentration factor only varied slightly with mesh refinement, as shown in Table A1 of the Appendix.

The fillet radius r at the corners of the slots was varied from half of the slot width down to 1/12th or 1/16th of the slot width, depending

Presented as Paper 2021-1805 at the AIAA SciTech Forum, Nashville, TN, January 11–21, 2021; received 29 April 2021; revision received 7 January 2022; accepted for publication 7 January 2022; published online XX epub-Month XXXX.

*Doctoral Student, Kevin T. Crofton Department of Aerospace and Ocean Engineering, Randolph Room 215, 460 Old Turner St.

†Professor and Interim Head, Kevin T. Crofton Department of Aerospace and Ocean Engineering, 460 Old Turner St. (MS 0203). Fellow AIAA.

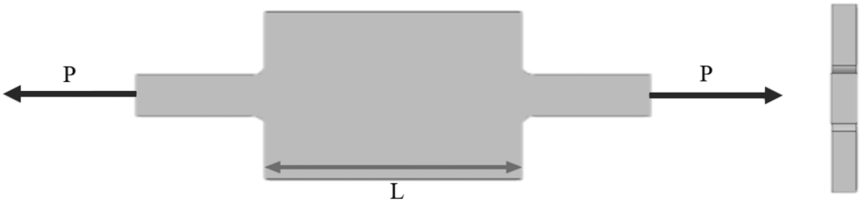

Fig. 1 Roark type 5 irregularity. Roark's type 5 irregularity, as shown within Roark's Table 17.1, is similar to the area between two slots on adjacent waveguides within an array [1].

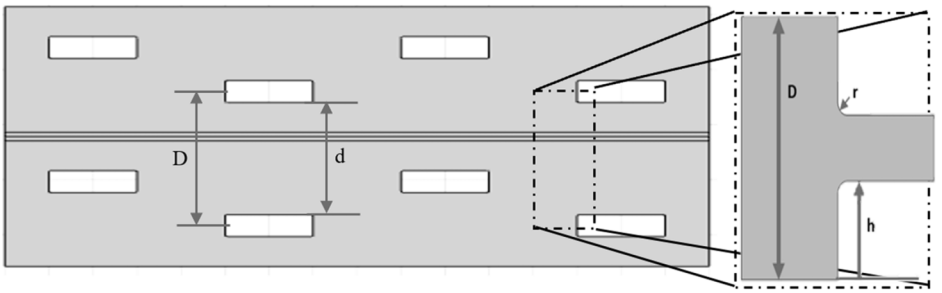

Fig. 2 Example waveguide array element. Roark's cases use the polynomial equation $K_t = C_1 + C_2(2h/D) + C_3(2h/D)^2 + C_4(2h/D)^3$, with the expansion on the right [1] similar to a subset of the waveguide array.

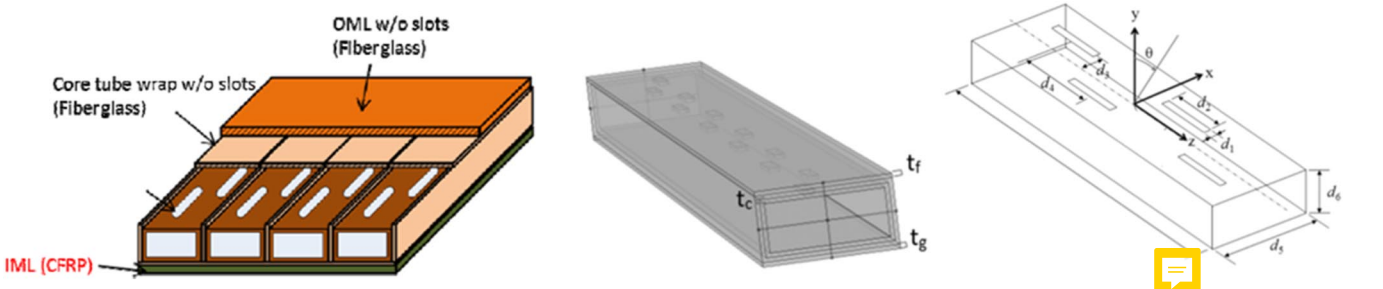

Fig. 3 Waveguide parameter definitions. The full waveguide with material locations is shown on the left, material thicknesses (t_f, t_c, t_g) in the center, and the additional waveguide and slot specific parameters ($d_1 - d_6$) on the right.

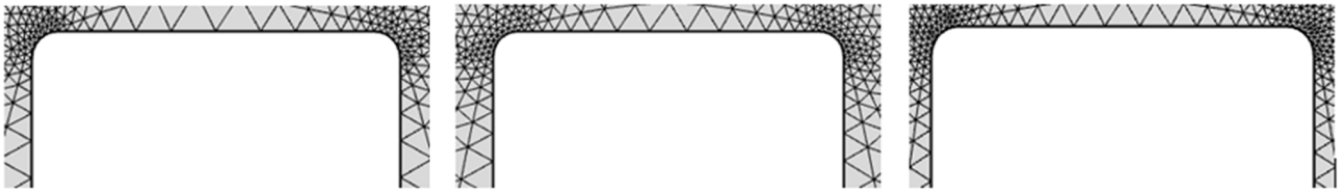

a) Fine mesh **b) Finer mesh** **b) Finest mesh**

Fig. 4 Mesh study grids. The mesh was varied to ensure proper coverage of the fillet curves.

upon the slot width's magnitude. This process was repeated for four slot widths, ranging from 1 to 4 mm, using a slot length of 10 mm. For each combination of slot size and fillet radius, the concentration factor is determined by dividing the von Mises stress at the corner node σ_{corner} by the nominal (applied) stress in the unreduced area σ_1.

$$K_t = \frac{\sigma_{\text{corner}}}{\sigma_1} \tag{1}$$

The von Mises stress was chosen for the isotropic material (copper in this case) failure criterion, due to it being more restrictive than the principal stresses alone. However, data was also taken for principal stress, as well as von Mises stress for both tensile and compressive loads to ensure the most conservative design. The data shown corresponds to the compressive von Mises case, as it was roughly equal to the tensile case and only slightly higher than the principal stress case. Figure 5 shows the data for each of the four designs modeled with a unit compressive load, labeled as COMSOL FEM data.

Curve fits were then created for the data collected from COMSOL [5] finite element models, with the overall goal being to find a general fit that could be used for any given ratio of radius over reduced area width r/d and slot spacing (unreduced area) width over reduced area width D/d. Initial attempts used polynomial forms similar to Roark, but power law curves were found to fit the data far better than pure polynomial forms. Various forms of the power law fit were tested, each with different dependencies upon D/d, until settling on the following bivariate form.

$$K_t = \left(A\left(\frac{D}{d}\right) + B\right)\left(\frac{r}{d}\right)^{\alpha} \tag{2}$$

The coefficients A and B, as well as the exponential α, were determined using a least-squares fit and resulted in the final form shown in Eq. (3), with an overall residual squared of $R^2 = 0.914$. The residuals for each case, along with the comparable univariate curve fits for each individual line, are contained within Table A2 of the Appendix.

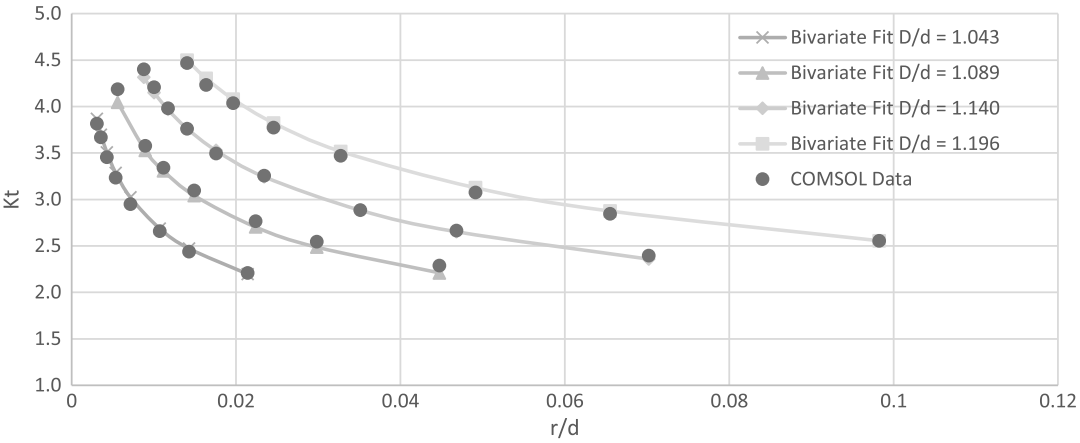

Fig. 5 COMSOL FEM data compared against bivariate fit for each D/d ratio of slot spacing to reduced-width data. Most cases track fairly well, with only one case slightly overestimating values and one case slightly underestimating values.

Table 1 Bivariate solution weakness. When either equation is applied to slots outside of its original data set, it loses accuracy

	10 mm slots		15 mm slots	
	Equation (3) R^2	Equation (4) R^2	Equation (3) R^2	Equation (4) R^2
$D/d = 1.043$	0.9834	0.9952	0.9216	0.9680
$D/d = 1.089$	0.9598	0.6062	0.9547	0.9381
$D/d = 1.140$	0.9860	0.2491	0.5576	0.9788
$D/d = 1.200$	0.9843	0.5251	0.0096	0.9616
Total	0.9135	−0.6243	−0.5565	0.8465

$$K_t = \left(3.7962\left(\frac{D}{d}\right) - 3.2394\right)\left(\frac{r}{d}\right)^{-0.2905} \tag{3}$$

The accuracy of the bivariate fit is of the same order of magnitude as the univariate fits for each parameter varied with the other fixed, while also allowing for more convenient estimation of intermediate points. Figure 5 shows how the trends for each D/d compared to the data themselves.

After validating the accuracy of the bivariate curve fit, additional data was included for a longer slot of 15 mm. However, the bivariate form in Eq. (3) no longer predicted the concentration factors accurately. Instead, with the exception of $D/d = 1.089$, the R^2 value of each data set dropped below 0.8. As a result, a new form the equation was derived from the 15 mm slot data for comparison. Its data regression led to the variables A, B, and α changing significantly as follows.

$$K_t = \left(4.354\left(\frac{D}{d}\right) - 3.841\right)\left(\frac{r}{d}\right)^{-0.2993} \tag{4}$$

Similarly, when Eq. (4) was used, it accurately predicted the concentration factors for its original data set, but failed to produce accurate results, as shown in Table 1.

As mentioned in Roark's text, the stress concentration exponentially decays toward unity as it moves away from the corner/hole [7]. The proximity of the nearby slots, which changed as a result of the lengthwise extension or contraction, likely explains the change in the equation's coefficient values, as well as the decrease in accuracy when applied to slots of different lengths. As a result, a third term was added to account for the influence of additional nearby slots and their corresponding stress concentrations. Additionally, the terms were now normalized by the unreduced area D to allow for consistent scaling within the equation, as the slot sizes and spacings were varied.

Multiple forms of the trivariate form were tested, with different inclusions of a new distance term s corresponding to the distance between the nearest corners. Various forms were tested, including adding the new term in a manner similar to the D/d term in Eq. (2), as well as multiplying or dividing Eq. (2) by the distance term. The best result came from the form shown in Eq. (5), where the middle term facilitates recovery of the original bivariate form as the distance between nearest corners approaches infinity.

$$K_t = \left(A * \left(\frac{d}{D}\right) + C\right)\left(1 + \frac{B}{\left(\frac{s}{D}\right)}\right)\left(\frac{r}{D}\right)^{\alpha} \tag{5}$$

Just as with the bivariate form, the coefficients for the trivariate curve fit were determined using a least-squares fit, but now for the entire data set of both 10- and 15-mm-long slots. The resulting Eq. (6) maintained a residual squared greater than 0.9 for all cases, with comparisons against the bivariate and univariate solutions for each data set shown within Table A3 of the Appendix.

$$K_t = \left(-4.262\left(\frac{d}{D}\right) + 4.712\right)\left(1 + \frac{0.0308}{\frac{s}{D}}\right)\left(\frac{r}{D}\right)^{-0.295} \tag{6}$$

Figures 6 and 7 show how the trivariate and bivariate curves compare against the 10 and 15 mm data points from the COMSOL models, respectively.

With the finalized trivariate form, a direct comparison to the nearest Roark form can be made. However, Roark's type 5 irregularity is not considered valid if the ratio between the unreduced area distance L and the slot separation distance D is too low, as governed by the inequality:

$$\frac{L}{D} \geq \frac{3}{\left[\frac{r}{D-2h}\right]^{1/4}} \tag{7}$$

Due to the slots within a waveguide being so close to one another, the equivalent L/D ratio falls below the threshold. Consequently, the residual for the Roark approximation was poor, varying between negative values of −0.089 and −11.36, whereas the trivariate fit had residuals varying between 0.90 and 0.99. The comparison is easier to see in Figs. A1 and A2 of the Appendix, which demonstrates how the Roark fit becomes less and less accurate as the D/d ratio increases. The bivariate and trivariate curve fits were also compared to *Peterson's Stress Concentration Factors*, which also fared poorly, because it too was found to be below its viability threshold [7].

III. Multifidelity Design Application of Bivariate Fit

With the bivariate and trivariate curve fit coefficients determined, the corner stresses can now be accounted for within an optimization procedure without requiring a finely remeshed finite element model

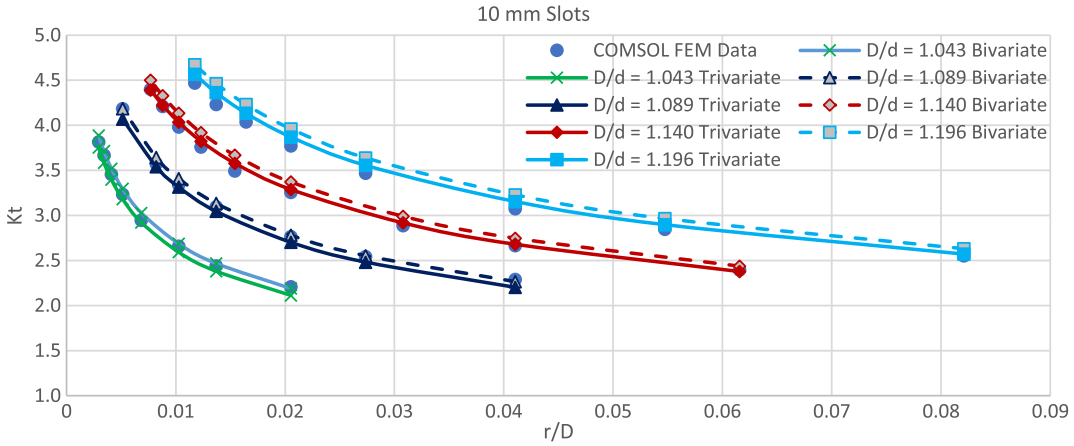

Fig. 6 Bivariate and trivariate fits for 10 mm slots. Both data sets track the two inner curves well, although the trivariate appears to be the more accurate of the two cases.

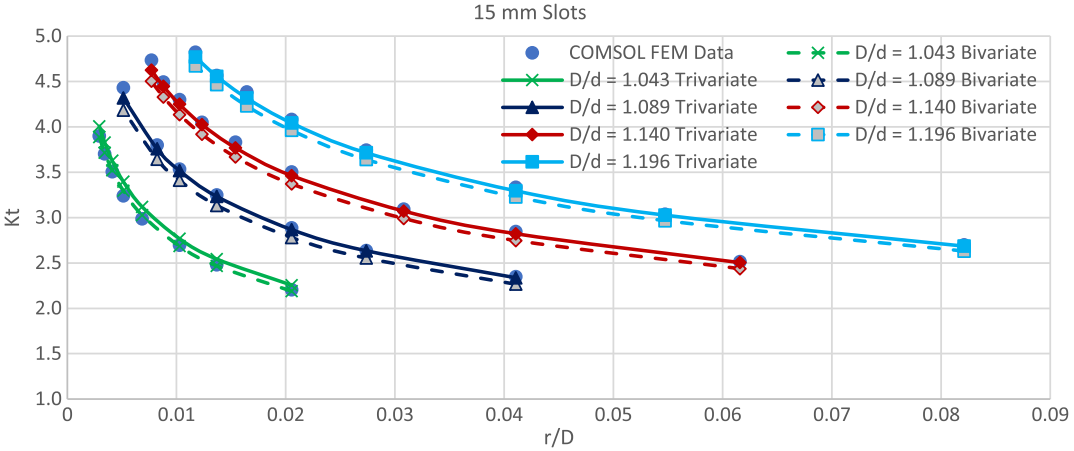

Fig. 7 Bivariate and trivariate fits for 15 mm slots. As with the 10-mm-length slots, the trivariate form appears to track better, but now appear to overestimate the lowest $D/d = 1.043$ line.

for each candidate geometry. Here, the waveguide optimization focuses on varying the slot width and centerline spacing, because the slot length is dictated by the target frequency and the lengthwise spacing by the desired radiation pattern. These two factors combine to determine the unreduced area width D and reduced area width d. Fillet radius was added as the final variable. The centerline spacing was constrained to ensure that slots do not overlap on a single waveguide. This leaves the slot width and radius as the driving forces for the optimization that accounts for these corner concentrations.

In practice, the embedded waveguides would be installed as panels in the aircraft's wing or fuselage skin, placing them between ribs on each end. Therefore, the in-plane compressive loads are applied uniformly across the end areas of three-dimensional models, or as an edge load in the simplified plate models, simulating skin compression as the wing bends due to flight loads. To realize practical design loads and stress limits for this example, estimated flight loads of the X-47B were used to test designs. The loads were calculated based upon the listed maximum takeoff gross weight of 44,000 lb and an assumed lift profile varying from linear on the narrowing inboard section to elliptical along the constant span outer section. The resulting moment distribution was consistent with the typical root-wing bending moment (RWBM) of about 10×10^6 lb-in for military class aircraft of this size. Next, based on the geometry of the X-47B wing [8], the RWBM was used to estimate a representative compressive load in the top skin panel. A 3 g load factor and a 1.5 factor of safety required that the designs withstand at least 19,400 Newtons (4340 lb) of load applied to the embedded antenna panel.

A mass minimization was conducted in MATLAB with a coarse FEM that neglected the slot fillet, using instead the bivariate fit to account for stress concentration, which was then verified in a higher-fidelity filleted FEM in COMSOL multiphysics. Within the optimization code, slot width d_1, slot centerline-offset d_3, waveguide height d_6, fillet radius r, and waveguide material thickness were all allowed to vary. Several geometric constraints were added to ensure the slots remained within the perimeter of the waveguide upper surface, whereas an additional constraint ensured that the fillet radius could not exceed half of the slot width, in addition to its side constraints. Another constraint ensured that the mass had to be less than the nominal mass. The final constraint ensured the stress at the corner of the slot did not exceed the yield stress of the copper given in Table 2. The corner stress was calculated by multiplying the

Table 2 SQP optimization results for a copper waveguide. The slots were expanded and the height and thickness reduced with buckling was not constrained, whereas constraining the buckling resulted in smaller slots and increased fillet radii

Variable	Nominal (mm)	Optimized without P_{cr} constraint (mm)	Optimized with P_{cr} constraint (mm)
d_1	2.00	3.00	1.30
d_3	2.00	2.10	2.20
d_6	10.16	8.00	9.30
r	0.200	0.900	0.630
t_c	0.750	0.500	0.710
	Objective & Constraint Values		
Mass (kg)	0.0867	0.0542	0.0810
Buckling load (N)	13,700	5,630	10,900
Max stress (MPa)	1055	544.9	550.0

concentration factor from the geometry against the stress in the unreduced area, with the applied load being calculated as the buckling load for the given waveguide geometry. The buckling load was calculated through Euler-column buckling modified by a Timoshenko shear reduction factor:

$$P_{\text{cr}} = \frac{P_e}{1 + \frac{\eta P_e}{AG}} \tag{8}$$

In Eq. (8), P_e represents the lowest eigenvalue of the standard beam buckling problem, A is the end area of the beam, G is the shear modulus of the beam's material, and η represents the Timoshenko shear coefficient, which is typically taken as $5/6$ [9].

The optimization was conducted using a MATLAB implementation [10] of sequential quadratic programming (SQP) [11] in conjunction with the bivariate form in Eq. (4), with the resulting design variable values shown in Table 2. Figure 9 shows the difference between the meshing of the high-fidelity COMSOL model and the low-fidelity MATLAB model. The waveguide height and thickness were both taken to their minimum values, whereas the slot width increased to its maximum value. With three of the five values at their extremes, the slot offset only varied slightly from its initial value at the minimum, and the fillet radius was decreased to the minimum value necessary to meet the stress constraint. The first tests conducted validated the original bivariate version of the curve fit, showing its viability, before implementing the additional modifications for the trivariate fit listed in the preceding section. The resulting design decreased the waveguide's mass by 37.4 percent, from approximately 0.0867 to 0.0542 kg, whereas the waveguide's buckling load decreased by 58.9 percent, from approximately 13,700 N to 5630 N.

The results indicate that the optimizer was removing as much mass as possible, with the reduction in height also having the added effect of reducing the applied buckling load and, as a result, the compressive stress in the waveguide. To combat this, a constraint was added to ensure the buckling load of the waveguide does not decrease beyond 80% of the original buckling load. The final column of Table 2 shows how this additional constraint resulted in a significant change in the optimized design. To meet the buckling constraint, the slot width was reduced, rather than increased, to provide additional stability. The fillet radius was limited by the constraint dictating that it cannot exceed half of the slot width, whereas a larger final thickness sustained the additional load. The resulting optimized design resulted in a mass decrease of 6.57%, from 0.0867 to 0.0810 kg, and the buckling load abiding by the 80% constraint, finalizing at 10,900 N.

A 12-slot waveguide model, with fillet radii 1/10th of the slot's width, was created in COMSOL to verify these designs, as shown in Fig. 8A. According to the approximate model, the copper waveguide should have a buckling load of 13,700 N and a concentration factor of 3.65 between the von Mises stress at the corner and the nominal compressive stress caused by a unit load. The COMSOL model for these nominal values determined that the buckling load was 13,200 N, a difference of only 3.65 percent. Additionally, stress patterns in Fig. 10A result in a stress concentration factor of approximately 3.22 at the corner. Whereas the prediction is in error relative to the FEM value by approximately 11.8%, it is worth noting that it is an overestimation of the concentration factor, resulting in more conservative designs that are likely stronger than required. The discrepancy likely stems from the design's lower r/D value, placing it in the region where the curve becomes more exponential and tends to overestimate concentration factor values.

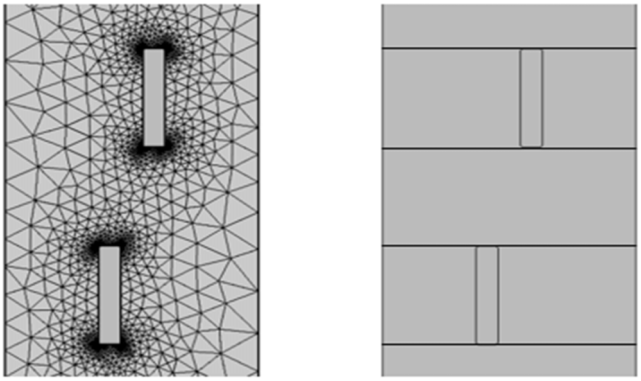

a) b)

Fig. 9 a) COMSOL mesh compared to b) low-fidelity design model mesh. The COMSOL mesh added many elements to fully capture the corner effects, whereas the fit allowed for the low-fidelity mesh to account for the corner stresses.

After verifying the accuracy of the curve-fit estimate of stress concentration with the nominal design, the optimized design was modeled next in COMSOL, as shown within Fig. 8B. The model chosen was the second result in Table 2, with the additional buckling constraint added. The COMSOL model predicted buckling would occur at 10,900 N, consistent with the constraint's estimate of 10,900 N. The estimate predicted a corner stress concentration factor was 2.21, which is in line with the stress patterns within Fig. 10B, which correspond to a concentration factor of 2.22. Although slightly less than the COMSOL model's, the estimate is still within 0.48% of the actual value. The bivariate fit was used in this case due to the slot lengths being fixed during the analysis. The weakness for varying slot lengths appeared afterward, when implemented in the larger optimization described next in Sec. IV.

IV. Multifidelity Design Application of Trivariate Fit with Composite Materials

With the curve fit's viability confirmed for the initial optimization for fixed slot length, the bivariate form was then implemented within an optimization procedure to simulate its intended use. However, problems with inaccuracy for varying slot lengths dictated a different curve fit for 15 mm slots. As an alternative, the trivariate form was developed and implemented within a multi-objective optimization for varying slot length. As shown in Fig. 3, the copper waveguide sits at the center of the design, with a supporting fiberglass sleeve around

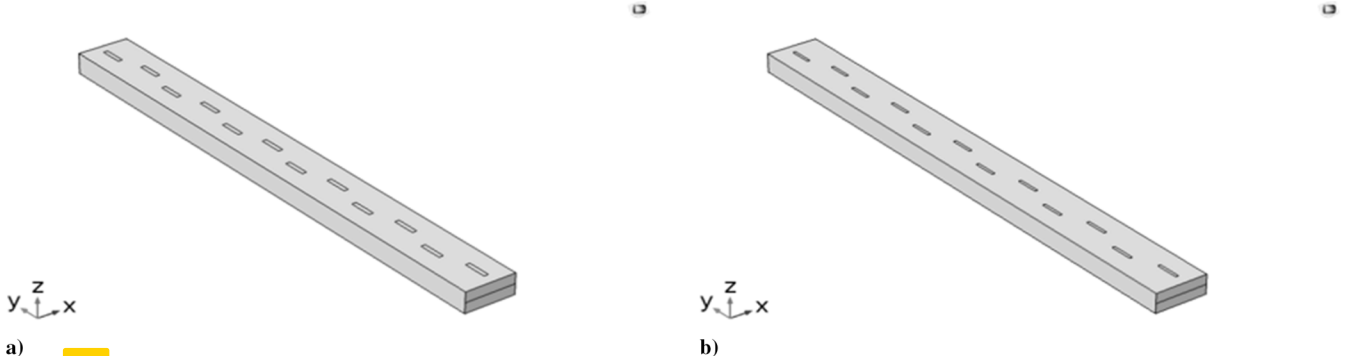

a) b)

Fig. 8 Waveguide configurations for a) nominal values, and b) optimized values. The nominal design shows the larger initial slots and their squarer shape, whereas the optimized design shows the narrowed and rounded slots.

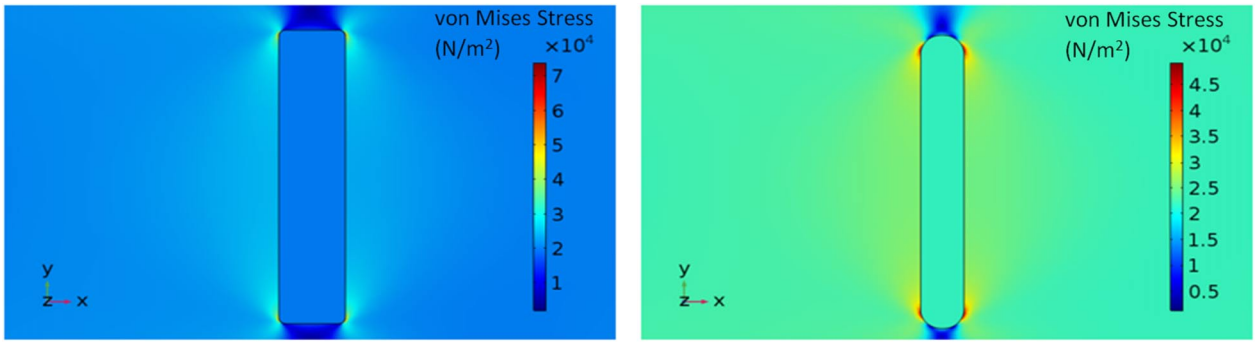

Fig. 10 Stress patterns for a) nominal slot dimensions, and b) optimized slot dimensions. The nominal design shows higher stress concentrations at the corners, whereas the optimized form has reduced their magnitudes to a level closer to the rest of the waveguide.

it, as well as an outer fiberglass face sheet covering the slotted waveguide and an inner graphite epoxy face sheet on the opposite side. Fiberglass was chosen due to its stiffness, but also because it is electromagnetically transparent and will allow radar transmission to be unhindered. Graphite epoxy was chosen for the inner face sheet due to its high stiffness and strength-to-mass ratio, allowing the design to increase in stiffness and strength at a reduced mass penalty. However, graphite epoxy is not electromagnetically transparent, resulting in it only being used on the inner face sheet where the impact on the electromagnetic performance is not a factor. Although these supporting materials are intended to bear a large portion of the load, proper modeling of the concentration factors around the slot corners allows the optimization to load the copper without ignoring the local yielding that would occur as a result.

The optimization performed with a range of weightings for minimizing the mass and maximizing the buckling load, while subject to constraints ensuring the designs are both physically feasible and do not result in failure of any of the materials. However, the inclusion of the concentration factor showed that the copper cannot support loading from the outset without either the mass or buckling load deteriorating. When the copper was loaded, designs resulted that were drastically heavier and weaker than an unloaded copper waveguide. With all of these factors combined, loading the copper from the start appears to be a significant restriction on the design process. As a result, the copper was left as an unloaded insert free to slide within the supporting fiberglass sleeve. The resulting designs, such as the one within Table 3, reduced the copper thickness to save on mass, which then allowed for the graphite epoxy and fiberglass thicknesses to be increased to strengthen the material without violating the mass constraint.

Table 3 Optimization of a full waveguide design. The reduction in mass from decreasing the copper thickness offsets the increase due to increasing the thickness of the supporting materials, while also increasing the overall buckling load

Variable	Nominal (mm)	Optimized (mm)
d_1	2.00	3.00
d_3	2.00	2.50
d_6	10.16	12.0
r	0.500	0.664
t_c	0.750	0.125
t_f	0.750	1.10
t_g	0.750	2.00
Objective and constraint values		
Total mass (kg)	0.162	0.108
Copper mass (kg)	0.109	0.0183
Buckling load (N)	36,680	100,300
Max fiberglass stress (MPa)	— —	421.9
Max graphite epoxy stress (MPa)	— —	999.5
Max copper stress (MPa)	— —	0

V. Future Work

The accuracy of the trivariate fit allows the concentration factors to be included in the design process and avoid overloading the copper waveguide. However, the analyses with the concentration factor limits showed that the copper could not be loaded from the offset without adversely affecting the resulting designs. Additional research is being conducted to implement the use of an initial offset, where the supporting material is extended beyond the end of the copper waveguide to prevent it from initially coming into contact with the loading surface. This offset will allow the supporting material to deform and absorb the majority of the loading, reducing the load seen by the copper waveguide to a value that will not result in local yielding at the slot corners.

VI. Conclusions

To properly analyze a loaded waveguide, it is important that the stress concentrations at the slot corners are properly modeled. In contrast to the initial polynomial forms used, analysis showed that a power law better fit the data, allowing both the initial bivariate and trivariate forms to accurately model the corner stresses using a coarser mesh. As a result, slotted waveguides can be analyzed with a simplified mesh, rather than the more complex meshes currently required to properly capture the curvature at the slot corners, or even simply with a hand calculation of the unreduced area's stress. The final trivariate form's slot-corner-distance term allowed the approximation to be used across multiple slot lengths, allowing for use within design optimization. The initial designs showed that the copper cannot be fully loaded from the start without a significant mass and buckling penalty.

Appendix

Table A1 Mesh refinement values. Finest mesh stress concentration factor converged to two significant digits

Mesh	Corner stress (N/m²)	K_t	Change from previous K_t (%)	Total elements
Fine	140,400	2.565	— —	4,212
Finer	145,200	2.653	3.317	5,322
Finest	143,400	2.620	−1.244	7,900

Table A2 Residuals for each D/d value. Global bivariate fit has a residual similar to the univariate models created for each individual model. With the overall accuracy of the same magnitude

	Univariate R^2	Bivariate R^2
$D/d = 1.043$	0.9985	0.9834
$D/d = 1.089$	0.9980	0.9598
$D/d = 1.14$	0.9981	0.9860
$D/d = 1.20$	0.9994	0.9843
Total	0.9940	0.9135

Table A3 Residuals for global fits for each D/d value. Bivariate fit is no longer able to maintain its accuracy for multiple slot lengths, with the inclusion of the slot-corner-distance term in the trivariate case recapturing the accuracy of the univariate fit

	10 mm slots			15 mm slots		
	Univariate R^2	Bivariate R^2	Trivariate R^2	Univariate R^2	Bivariate R^2	Trivariate R^2
$D/d = 1.043$	0.9985	0.9765	0.9651	0.9984	0.9942	0.9047
$D/d = 1.089$	0.9980	0.9887	0.9661	0.9994	0.8609	0.9843
$D/d = 1.14$	0.9981	0.8640	0.9833	0.9996	0.8058	0.9766
$D/d = 1.20$	0.9994	0.7590	0.9378	0.9996	0.8979	0.9884
Total	0.9940	0.5882	0.8523	0.9970	0.5588	0.8539

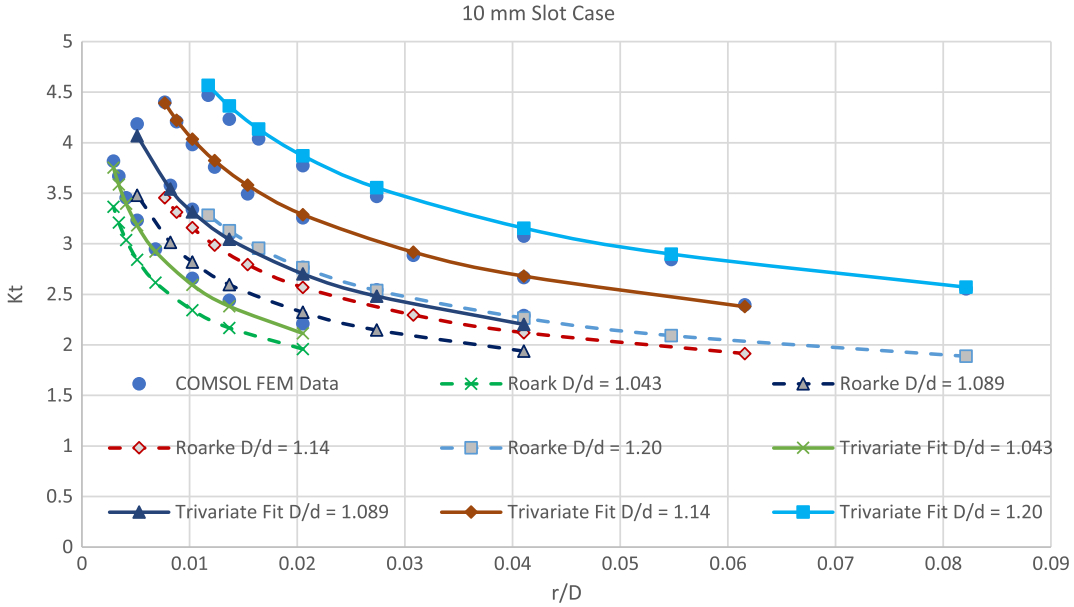

Fig. A1 Roark type 5 irregularity vs. trivariate fit for 10 mm slots. As the D/d ratio increases, Roark's fit becomes less and less accurate, whereas the trivariate fit maintains its accuracy throughout.

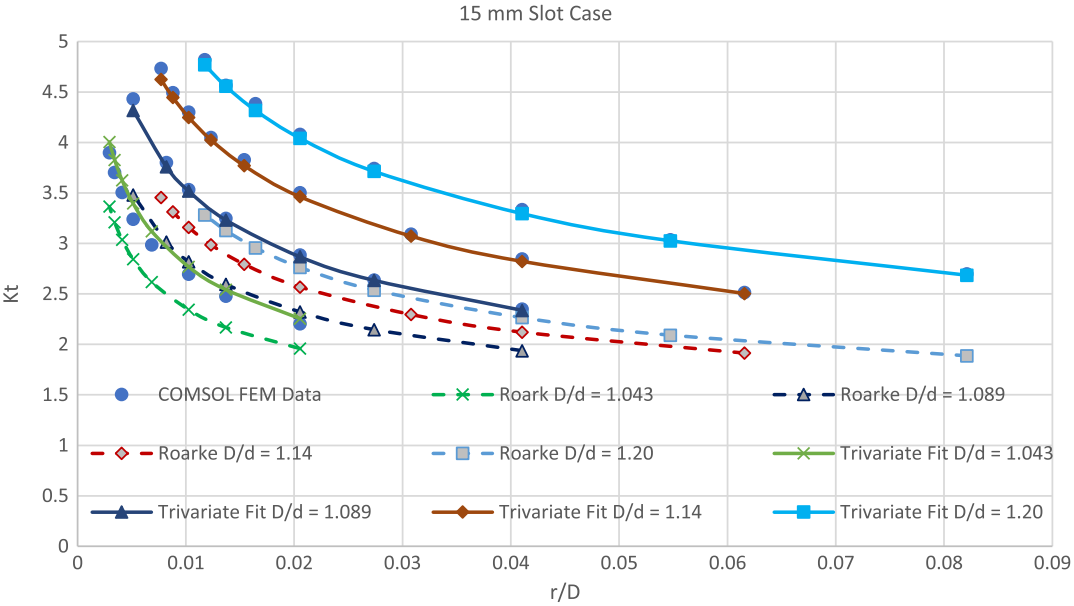

Fig. A2 Roark type 5 irregularity vs trivariate fit for 15 mm slots. Just as with the 10 mm slots, Roark's fit decreases in accuracy as D/d increases, whereas the trivariate fit maintains its accuracy throughout.

References

[1] Young, W., Budynas, R. G., and Sadegh, A., *Roark's Formulas for Stress and Strain*, 8th ed., McGraw-Hill, New York, 2011, p. 812.

[2] Kim, W., Canfield, R. A., Baron, W., Tuss, J., and Miller, J., "Structural Design and Optimization of Slotted Waveguide Antenna Stiffened Structures Under Compressive Load," *Carbon-Related Materials in Honor of Nobel Laureate Akira Suzuki's Lecture at IUMRS-ICEM 2018*, edited by C. Miron, P. Melo, S. Kaneko, and T. Endo, Springer International Publ., 2020.
https://doi.org/10.1007/978-3-030-44230-9

[3] Ha, T., and Canfield, R. A., "Design Optimization of a WR-90 Slotted Waveguide Antenna Stiffened Structures," *52nd AIAA/ASME/ASCE/AHS/ASC Structures, Structural Dynamics and Materials Conference*, AIAA Paper 2011-2147, April 2011.
https://doi.org/10.2514/6.2011-2147

[4] Kim, W., Canfield, R. A., Baron, W., Tuss, J., and Miller, J., "Modeling and Simulation of Slotted Waveguide Antenna Stiffened Structures," *19th International Conference on Composite Materials*, 2013.
https://doi.org/10.1007/978-3-030-44230-9_4

[5] COMSOL Multiphysics, Software Package, Ver. 5.2a, COMSOL Inc.

[6] Young, W., Budynas, R. G., and Sadegh, A., *Roark's Formulas for Stress and Strain*, 8th ed., McGraw-Hill, New York, 2011, pp. 800–803.

[7] Pilkey, W. D., *Peterson's Concentration Factors*, 2nd ed., John Wiley & Sons, New York, 1997, p. 151.
https://doi.org/10.1111/j.1475-1305.1998.tb01083.x

[8] Ortega, T. J., "X-47B UCAS Unmanned Combat Air System," Northrop Grumman Systems Corporation, San Diego, Aug. 2015, https://www.northropgrumman.com/wp-content/uploads/UCAS-D_Data_Sheet.pdf [accessed 1 July 2022].

[9] Timoshenko, S., and Gere, J., *Theory of Elastic Stability*, 2nd ed., Dover Publications, New York, 1989, p. 133.

[10] Canfield, R. A., "Quadratic Multipoint Exponential Approximation: Surrogate Model for Large-Scale Optimization," *Advances in Structural and Multidisciplinary Optimization*, Springer International Publishing, 2017, pp. 648–661.
https://doi.org/10.1007/978-3-319-67988-4_49

[11] Schittkowski, K., "NLPQL: A FORTRAN Subroutine Solving Constrained Nonlinear Programming Problems," *Annals of Operations Research*, Vol. 5, 1986, pp. 485–500.
https://doi.org/10.1007/BF02739235

C. Pettit
Associate Editor

Queries

1. AU: Please check that the copyright (©) type is correct. Please note that the code will be added upon publication.
2. AU: Please note that AIAA does not use commas or parentheses around a term that immediately follows its definition.
3. AU: Please review Ref. [4], as it specifies more than two authors, and was therefore changed to "et al." in text. Please confirm this is correct, or edit further as necessary.
4. AU: Please note that AIAA reserves capitalization for proper names and acronyms (not acronym definitions).
5. AU: Please define the acronyms in Fig. 3 and add them to the caption.
6. AU: Please review and edit the sentence beginning with "As a result" for clarity.
7. AU: Please review the book title in text for Ref. [7], as it differs slightly than that shown in the reference list. Please edit further as necessary.
8. AU: Please note that AIAA requires acronyms be used more than once to remain in the paper.
9. AU: As AIAA requires the figures to be cited in the order in which they appear in the main text, please reorder and renumber the figures accordingly.
10. AU: Please provide a descriptive title for the Appendix.
11. AU: For Ref. [2], please provide the location of the publisher and the pages if citing specific pages.
12. AU: If Ref. [4] is a published proceedings, please provide the full name and location of the publisher (NOT of the conference host) and the page range. If it is a conference paper, please provide the paper number and the organizer's name.
13. AU: For Ref. [5], please provide the location of the publisher and the year.
14. AU: Reference [6] was not cited in the main text. Please cite the reference in the main text (which does not include the Conclusions section, figures, or tables) in numerical order or remove the reference.
15. AU: For Ref. [10], please provide the location of the publisher.
16. AU: Please provide the issue number and/or month of publication for Ref. [11].

Funding Information

No funding information available.